

Energy equilibration in composite nuclei at high energy and spin: Correlations between evaporative ^1H , ^4He , and fission

M. F. Rivet*

*Department of Chemistry, State University of New York at Stony Brook,
Stony Brook, New York 11794*

D. Logan

Department of Chemistry, Carnegie-Mellon University, Pittsburgh, Pennsylvania 15213

John M. Alexander, D. Guerreau,* and E. Duek

*Department of Chemistry, State University of New York at Stony Brook,
Stony Brook, New York 11794*

M. S. Zisman

Lawrence Berkeley Laboratory, Berkeley, California 94720

Morton Kaplan

Department of Chemistry, Carnegie-Mellon University, Pittsburgh, Pennsylvania 15213

(Received 2 June 1981)

Correlations have been studied between evaporative H/He emission and fissionlike products for the reactions 333 MeV $^{40}\text{Ar} + ^{116}\text{Sn}$, ^{154}Sm , and ^{197}Au . Fission products were detected at 60° and 320° in coincidence with H and He at 120° in plane and 27° and 60° out of plane. The coincidence energy spectra of H and He are not consistent with evaporation from the moving fragments. An analysis has been made with the assumption of complete energy equilibration in the particle emission (i.e., evaporation) prior to scission. The rather large data set is essentially consistent with this assumption. From the spectral shapes one can deduce level density parameters and barriers to evaporation. Values inferred for the Fermi gas level density parameters are similar to those inferred from experiments at much lower energies. Values deduced for the emission barriers are much smaller than those from systematics of fusion barriers. The observed cross sections for fission and ^1H and ^4He evaporation are not easily reconciled with statistical model calculations. In particular, the proton evaporation seems to compete more favorably with fission and ^4He evaporation than implied by phase space considerations alone.

NUCLEAR REACTIONS $^{116}\text{Sn}, ^{154}\text{Sm}, ^{197}\text{Au}(^{40}\text{Ar}; \text{H/He, fission})$, $E = 333$ MeV, measured energy and angular correlations of evaporative H/He in coincidence with fission. Values deduced for emission barriers, temperatures and J_{rms} for the emitter. Comparisons made to evaporation calculations.

I. INTRODUCTION

Is it valid to assume that equilibrium has been achieved among specified degrees of freedom? This is a primary question for the understanding of any class of reactions. In the interactions between complex nuclei one can build composite systems with

enormous excitation energies and angular momenta. We must carefully test how far one can extend the assumption of equilibration in order to reduce the number of important variables to a manageable level.¹

In deeply inelastic reactions between complex nuclei, products are observed with extremely large en-

ergy damping but with masses rather similar to the original projectile and target.² The relatively small net mass changes accompanying these large energy changes suggest a slow approach to mass equilibration but a rapid approach to energy equilibration. Fission (or fissionlike) reactions are also abundant in heavy ion reactions; these produce a broad product distribution centered about half the mass of the fissile system. Clearly, extensive mass flow has occurred in such reactions, and it is possible that they occur subsequent to the formation of a completely equilibrated compound nucleus.

One group of these fissionlike reactions has attracted special attention in recent years as it may provide a bridge between the compound-nucleus concept and the double-nuclear concept used for deeply inelastic reactions.^{3,4} This group is characterized by apparent fission cross sections that are very large and demand the participation of many entrance-channel l waves $[(\sigma_{\text{fusion}}/\pi\lambda^2)^{1/2} \text{ or } l_{\text{crit}} > 100]$.⁴ According to the rotating liquid drop model (RLDM), an intermediate compound nucleus would have no barrier to fission for spins greater than ≈ 80 .⁵ The fissionlike nature of these reactions resembles the breakup of long-lived compound nuclei, but RLDM theory implies that their lifetimes should be very short.

Norenberg and Riedel, Gregoire *et al.*, and Swiatecki³ have suggested that these reactions proceed in two stages: (1) A double nuclear system is formed by the capture of the reactants inside a pocket or on a plateau in the potential appropriate to the entrance channel. (2) This double-nuclear system is able to execute more than one-half a rotation during the period of mass flow that leads to the final fissionlike products. This picture is in contrast to that of a compound nucleus which derives its long lifetime from the time for the totally equilibrated complex to concentrate energy in one decay mode.⁶

In this study we explore the extent of thermal equilibration in this interesting class of reactions. Three cases were chosen: 333 MeV $^{40}\text{Ar} + ^{197}\text{Au}$, ^{154}Sm , and ^{116}Sn ; other studies have shown that l_{crit} values are 143, 137, and 112, respectively,^{7,8} and that there is extensive emission of H and He prior to scission.^{9,10} Thus we can use this H/He emission as a probe of the extent of equilibration as the system evolves toward fission. If the picture of Ref. 3 is correct, a true compound nucleus is never formed (save for the lowest l waves) and therefore the extent of energy thermalization cannot be anticipated.

The tools that we use are the spectra of H and He

at backward angles and their correlations with fissionlike products. The direction of the fission product and the beam define a reaction plane that is expected to be nearly perpendicular to the angular momentum of the fissile system. The statistical model provides equations that describe the correlations expected between the spin vector and evaporated particles if equilibrium is achieved in the intrinsic particle motions.¹¹⁻¹⁶

Our conclusions are that most of the energy and angular distribution data, from both singles and coincidence studies, can indeed be accounted for by equilibrium theory with reasonable values for the temperature and moment of inertia of the emitting system, provided that one uses very small evaporation barriers.¹⁷ A notable exception is the ratio of cross sections for proton to alpha-particle evaporation to fission.¹⁸ A reasonable interpretation of the discrepancies is that the thermalization of the particle motions and their subsequent evaporation proceed much more rapidly than the collective motion toward equilibrium shapes. Therefore, the statistical theory for particle evaporation can retain much of its validity even though the collective motions may never lead to compound systems with shapes characteristic of the equilibrium theory for a liquid drop.⁵

II. EXPERIMENTAL ARRANGEMENT AND RESULTS

A beam of 334 MeV ^{40}Ar was produced by the Lawrence Berkeley Laboratory SuperHILAC. It was defined by two four-jaw collimators before entry into the 75 cm scattering chamber and then monitored by a Faraday cup and two Si detectors fixed at small angles on either side of the beam axis. Self-supporting targets were used of ^{197}Au , ^{154}Sm , and ^{116}Sn ; the thickness of the Au target was determined by weight and by α -particle energy-loss measurements; the others were measured relative to it by elastic scattering. Fissionlike products were detected in two gas ionization telescopes (GT) (≈ 20 Torr of methane and 300 μm Si stopping detector) with solid angle acceptance of ≈ 1 msr.¹⁹ Light charged particles (H/He) were detected in three solid state telescopes (SST) (each with 45 μm , 500 μm , and 5 mm Si detectors) with solid angle acceptance of ≈ 6 msr. Cover foils of ≈ 10 mg/cm² Pb were used for each SST; the resulting lab energy thresholds were ≈ 2 MeV for ^1H and ≈ 8 MeV for ^4He . Energy calibrations for each Si detector were made by reference to α decay from ^{212}Pb . Solid an-

gle determinations were made by geometry measurements and by the measured rates from calibrated sources of α radioactivity mounted at the target position.

The angular geometry of the scattering chamber is defined by spherical coordinates consisting of an "in-plane" angle ($0^\circ - 360^\circ$) with respect to the beam θ , and an out-of-plane angle ($0^\circ - 90^\circ$) φ . The actual laboratory angle with respect to the beam is a function of both θ and φ . We use subscripts G and S for these angles to denote GT and SST (and also f , p , or α to denote fission products, protons, or alpha particles, respectively). The angle in the c.m. system with respect to the beam is denoted by $\theta_{c.m.}$ and that with respect to the angular momentum vector of the emitter is $\varphi_{c.m.}^*$. (Note that $\varphi=0^\circ$ defines the reaction plane; this plane is approximately normal to the initial spin and therefore corresponds to $\varphi_{c.m.}^* \approx 90^\circ$.)

For this experiment we placed the detectors in one fixed configuration. The two gas telescopes for fissionlike products were both in plane ($\varphi_G=0$) with θ_G of 60° and 320° (i.e., 40° on the opposite side of the beam). The three solid state telescopes for H and He were mounted at $\theta_S=120^\circ$ with $\varphi_S=0^\circ$, 27° , and 60° . We have recorded on magnetic tape the pulse heights corresponding to coincidences between H or He and fission, along with those in the singles mode. The singles from each telescope were prescaled by a factor of 100. For each coincidence, the time delay between the signals from a GT and an SST was measured by a separate time to amplitude converter (TAC). The TAC spectrum had a peak of about 20 nsec width and a flat tail used to correct for random coincidences. Dead time for each telescope was measured by a pulser triggered by one of the beam monitors and passed through the test input of the preamplifiers.

In the figures we give vector diagrams to indicate the angles θ_G and θ_S ; and we label the out-of-plane angles by φ and/or by $\varphi_{c.m.}^*$. In Table I we list the cross sections and mean energies for H or He as measured in coincidence between a GT and an SST. The measurement of singles and coincidence events during the same experimental run provides very good precision for their comparison. The difference between the mean energies of H or He in coincidence and in singles gives a useful test of the equilibrium theory. Similarly, the reproducibility of the singles cross sections in each GT and SST provides a useful monitor of the reliability of each telescope. These singles cross sections for the fissionlike events are also given in footnote b to Table

I. Multiplicities (M_α or M_p) given in some of the figures are simply the ratios of coincidence to singles cross sections.

One of the angles chosen for the GT (60°) was much larger than the grazing angle for each target²⁰ and therefore very few projectilelike fragments were observed. However, a distinct peak was visible for the targetlike fragments which we have eliminated by applying gates to the ΔE and E signals. For the other GT angle (320°), projectilelike fragments were observed but were separated from fissionlike fragments in the same way. Gates on ΔE and E were used to define "fissionlike" fragments and no further Z identification was made.

It is of great importance to know if the coincidence requirement selects out some special class of the fissionlike products. In Fig. 1, ΔE - E contour maps are shown for fissionlike fragments from the Au target as recorded in singles and coincidence modes. The basic patterns are indeed very similar. However, a careful look shows that the events from the singles mode are richer in fissionlike fragments with relatively low ΔE and E (note the small peak at $\Delta E \approx 26$, $E \approx 6$). This effect is possibly more easily visible in the E cuts shown in the lower part of Fig. 1. We ascribe this to a small admixture (possibly a few percent) of sequential fission after small mass transfer from projectile to target. This sequential fission would arise from a composite system of lower Z and excitation energy. Therefore, the detected fragments would have lower Z and kinetic energy and fewer evaporated H and He would be expected to be seen in coincidence. This effect was not observed in the ΔE - E maps for ^{154}Sm or ^{116}Sn targets. Another simple way to look for selectivity by the coincidence requirement is to compare the energy distributions of the events recorded in singles and in coincidence. Figure 2 gives such a comparison for the ^{154}Sm target; similar results were obtained for ^{197}Au and ^{116}Sn . For the GT at 60° the ratio of singles to coincidence events is very nearly constant over the whole range of energies. As one knows that the light fragments have higher kinetic energies, a constant ratio indicates a lack of mass selectivity due to the coincidence requirement. For the GT at 320° the coincidence events seem to be less abundant for both wings of the energy (and therefore mass) distribution. As this effect seems significant only for the wings of the spectrum we may proceed with the knowledge that the coincident events derive from a reasonably representative sample of the fissionlike events. At first we were somewhat dismayed by the

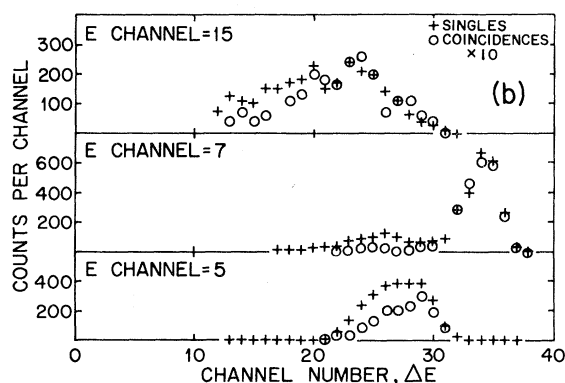
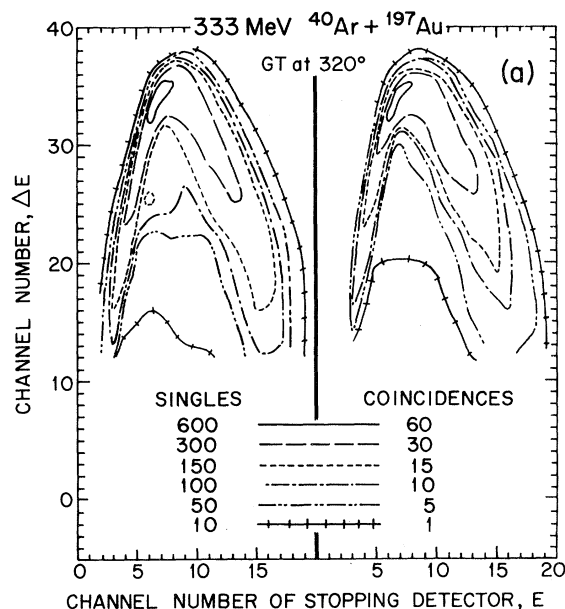


FIG. 1. (a) ΔE - E maps for fissionlike fragments (gates set on ΔE and E) recorded in the GT ($\theta_G = 320^\circ$) for 333 MeV $^{40}\text{Ar} + ^{197}\text{Au}$. Results from the singles mode are compared to those for coincidences with H or He detected at $\theta_S = 120^\circ$. (b) E cuts from these maps show slight differences attributable to a small admixture of sequential fission in the singles.

comparison of the shapes of the spectra at 60° to those at 320° . The flat shape at 60° , even at low energies, made us apprehensive. However, we see very similar shapes for calculated spectra from a Monte Carlo kinematic simulation of these fission processes and therefore we feel that it is the natural outcome of the velocity vector additions in fission following fusion.

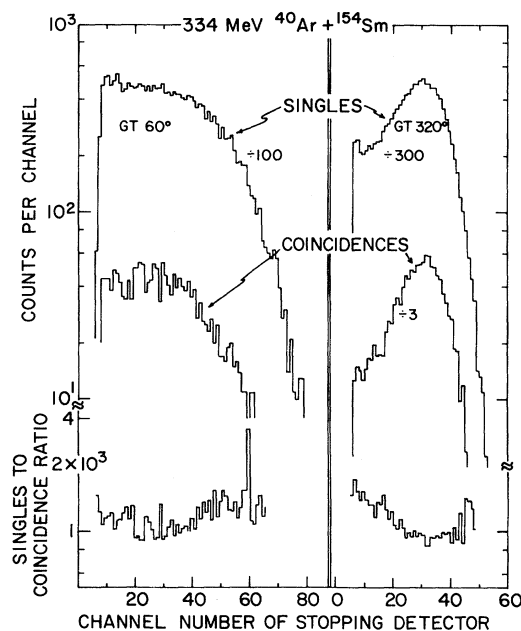


FIG. 2. Energy spectra for fissionlike fragments (gates set on ΔE and E) recorded in the GT for 334 MeV $^{40}\text{Ar} + ^{154}\text{Sm}$. The upper histograms are from the singles mode; the center ones are for coincidences with H or He detected at $\theta_S = 120^\circ$; the lower ones are the ratio of singles to coincidence.

III. DISCUSSION

A. Does H/He emission occur prior to or after full acceleration of the fission fragments?

In several earlier papers we have discussed a variety of evidences for H/He emission predominantly prior to scission.^{7,8,10} Even though the experiment reported here was designed primarily to measure out-of-plane correlations, it also provides a detailed means to search for the kinematic shifts characteristic of evaporation from fully accelerated fragments. Figures 3–6 show histograms of the measured coincidence spectra compared to curves calculated by a Monte Carlo simulation of evaporation from the moving fragments.

For this calculation we have assumed that the angular distribution of the fission fragments is proportional to $1/\sin\theta_{c.m.}$. (This assumption is not crucial because the coincidence requirement fixes the fission-fragment angles.) We also assume that the average total kinetic energy (TKE) released in fission is given by the Viola systematics²¹ (for all

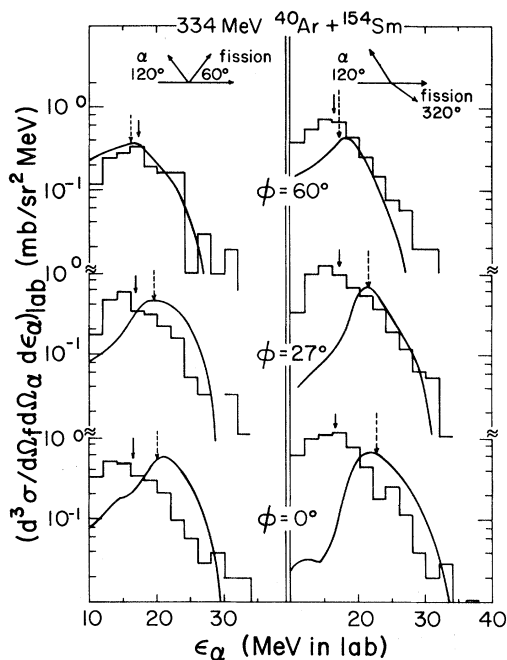


FIG. 3. Histograms for measured laboratory spectra of ^4He detected in coincidence with fission. The reaction and the geometry are indicated. Smooth curves were calculated by a Monte Carlo kinematic simulation of evaporation from moving fission fragments (see text). The solid and dashed arrows indicate mean energies for observed and calculated spectra, respectively.

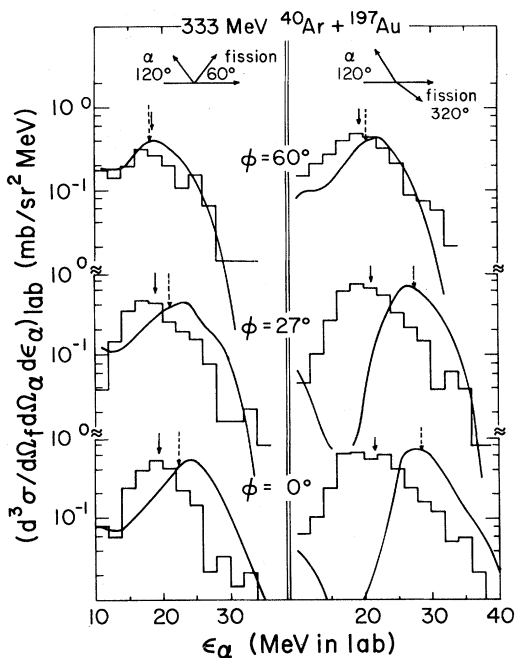


FIG. 4. Same as Fig. 3.

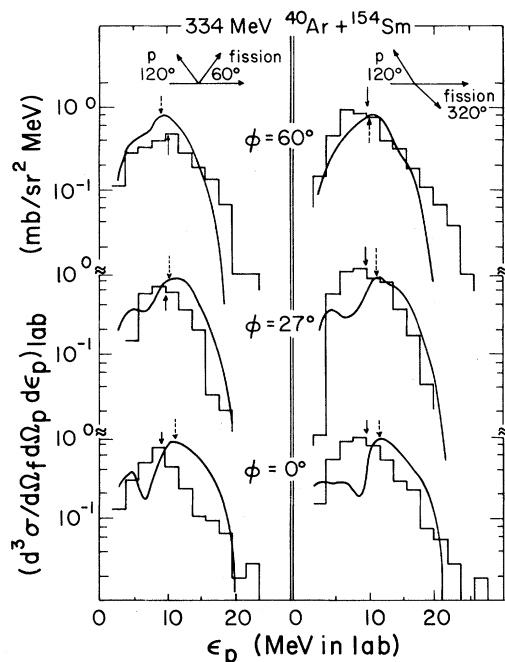


FIG. 5. Same as Fig. 3 but for ^1H .

masses), and the distribution of TKE is a Gaussian with standard deviation (σ_{TKE}) of 15 MeV.²² Standard deviations of the mass distributions (σ_A) were taken as 30, 24, and 25 for Au, Sm, and Sn, respectively.^{4,23} In the frame of the moving fragments the

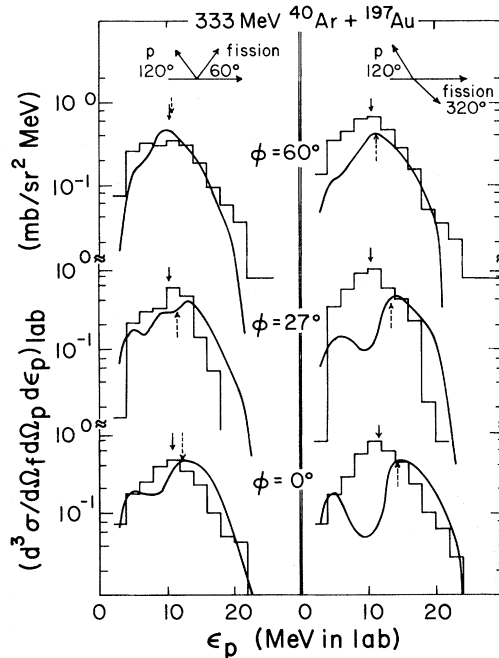


FIG. 6. Same as Fig. 5.

evaporation spectrum $P(\epsilon)$ was taken to be isotropic and of the form

$$P(\epsilon) \propto (\epsilon - B) \exp(-\epsilon/T') \quad (1)$$

with $T' = 2.0$ MeV and B taken from Ref. 17. The angular distribution of H or He was taken to be isotropic in the frame of the moving fragment. (The sticking condition would imply that the fragments are ejected with mean spins $\lesssim 20$ and hence would give essentially isotropic evaporation.²⁴)

Look particularly at the right hand sides of Figs. 3–6; the in-plane geometry places the SST, for $\varphi = 0^\circ$, at about 30° to the direction of the undetected fission fragment. Therefore, a substantial kinematic shift is expected here as evidenced by the large mean energy for the calculated curve. Lower calculated energies are expected as one increases the angle between the SST and the fission fragment—either by increasing φ to 27° or 60° or by changing the GT to $\theta_G = 60^\circ$. These systematic shifts in energy, as shown by the calculated curves, do not appear (as a primary aspect) in the measured histograms. This supports our earlier reported results for several in-plane angles (see Fig. 6 of Ref. 7), which similarly showed no evidence for major kinematic energy shifts. In addition, the energy spectra of ^4He observed in singles at backward angles are much narrower than expected for evaporation from fully accelerated fission fragments. These combined observations imply that only small fractions of the H/He emission at backward angles could be due to evaporation from fission fragments ($< 20\%$ for ^4He , $< 30\%$ for ^1H). In Refs. 7–10 other arguments have been presented based upon measurements of mean particle energies and the ratios of ^4He to ^1H emission, and these indicate that most emission occurs even prior to scission.

B. Is there evidence for emission from the neck between the separating fragments?

In fission at low excitation energies one observes ^4He and other light particles emitted nearly perpendicular to the direction of the fragments.²⁵ These are usually referred to as emission from the neck even though recent calculations may bring this notion into question.²⁶ Nevertheless, it is reasonable to ask if there is evidence for an angular correlation favoring emission perpendicular to the separation axis of the fragments. In Fig. 7 we have collected the in-plane coincidence cross sections from Refs. 7–9 along with the data from this work. Even

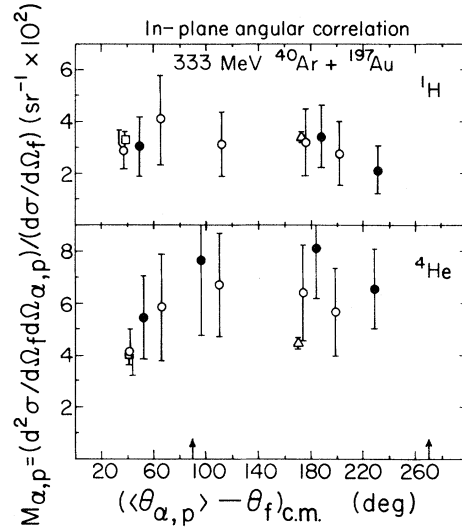


FIG. 7. In-plane angular correlations reported in Ref. 9 (circles) and this work [60° (squares) and 320° (triangles)] for ^1H and ^4He . Solid circles are for $\theta_G = 40^\circ$ and open points for $\theta_G = 60^\circ$.

though the statistics are generally rather poor, there is no evidence for strong preferential emission at 90° .

In Ref. 7 we discussed the possibility that emission might occur perpendicular to the separation axis but during the rotation period prior to scission. In this case the in-plane preference for 90° and 270° would be lost and preferential emission would be out of plane. There was some suggestion that ^1H emission might exhibit this out-of-plane preference. The data obtained here (see Table I and Figs. 10 and 11) show a preference for in-plane emission in each case, and we therefore discard this possibility for these reactions.

C. If we assume evaporation from a thermally equilibrated composite nucleus, what are its properties?

In Refs. 7 and 10 we showed that the shapes of the H and He energy spectra in singles become essentially independent of angle for $\theta_{\text{c.m.}} \gtrsim 100^\circ$. Also, their angular distributions show a slight increase with increasing $\theta_{\text{c.m.}}$ (toward $\theta_{\text{c.m.}} = 180^\circ$). These are the classic features of evaporation from a thermally equilibrated system and suggest that equilibrium theory may be applicable.^{11,12} In Figs. 8 and 9 we show some spectra for ^4He , measured in singles and coincidence and transformed to the c.m. system (see Appendix B). The spectra are very

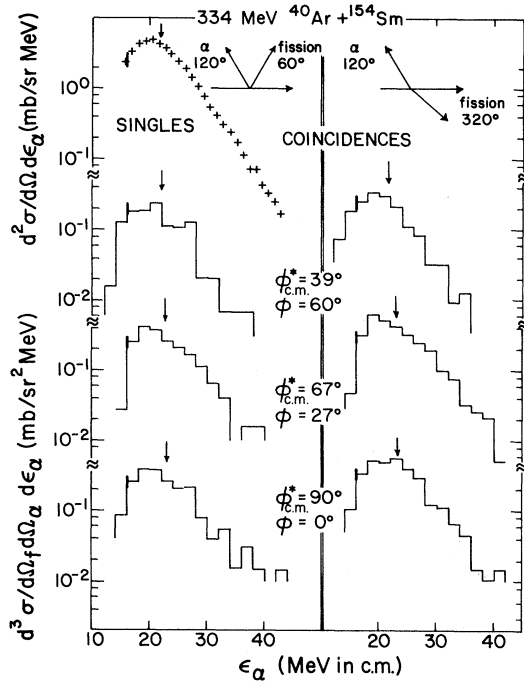


FIG. 8. Histograms of the observed c.m. energy spectra for ${}^4\text{He}$ in coincidence with a fission product. The laboratory out-of-plane angle φ is noted along with φ^* , the c.m. angle with respect to the spin vector. Singles spectra are noted by crosses. Arrows note the mean energies determined with a low-energy cutoff of 16 MeV as shown by the heavy vertical mark.

similar but show a slight decrease in mean energy with increasing out of plane (φ). This is also a feature of evaporation theory.

Let us review or develop the equations needed

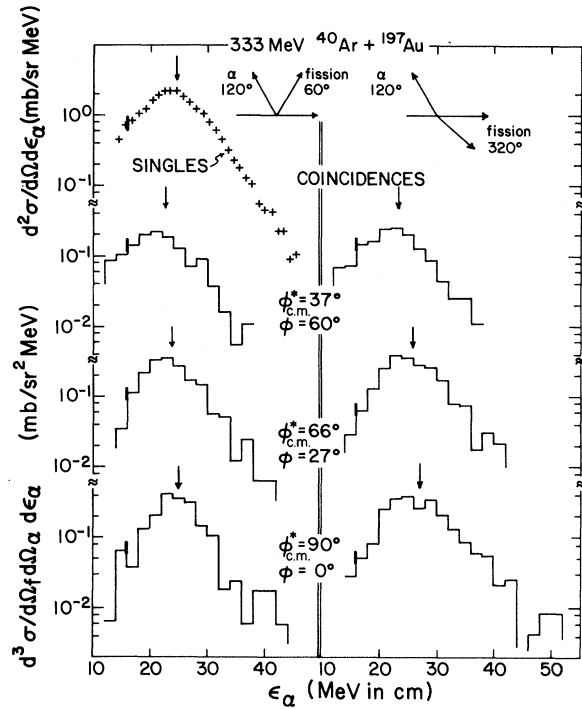


FIG. 9. Same as Fig. 8.

from evaporation theory and apply them to these data. Døssing has worked out some of them¹⁴ and we have extended this approach. He writes a general expression for the probability $P_i(E_0, J_0, \varphi_{\text{c.m.}}^*)$ of particle evaporation at angle $\varphi_{\text{c.m.}}^*$ with respect to the spin of an emitter with initial excitation energy E_0 and spin J_0 :

$$P_i(E_0, J_0, \varphi_{\text{c.m.}}^*) \propto \int_{l=0}^{\infty} \int_{\epsilon=0}^{\infty} T_{il}(\epsilon_i) \rho(E_0 - S_i - \epsilon_i, J_0, l) I_0(2\beta_1 \sin \varphi_{\text{c.m.}}^*) d\epsilon dl. \quad (2)$$

Here, $T_{il}(\epsilon)$ denotes the transmission coefficient for particle i with exit channel orbital angular momentum l and separation energy S_i . In this expression $I_0(\beta_1 \sin \varphi_{\text{c.m.}}^*)$ is the modified Bessel function found by Ericson and Strutinski¹² to describe the angular correlation for each emission characterized by a given value of β_1 ,

$$\beta_1 = \frac{\hbar^2(J_0 + \frac{1}{2})(l + \frac{1}{2})}{2\mathcal{J}T}. \quad (3)$$

Døssing has used the constant temperature level density expression $\rho(E, J)$ (expanded around the most populated energy and spin, E' and J' , in the residual nucleus) and the sharp cutoff transmission coefficients:

$$\rho(E, J) = \frac{(2J+1)}{(2J'+1)} \rho(E', J') \exp \left\{ \frac{1}{T}(E - E') - \frac{\hbar^2}{2\mathcal{J}T} [J(J+1) - J'(J'+1)] \right\} \quad (4)$$

and

$$T_l(\epsilon) = \begin{cases} 0, & \text{for } \epsilon < B + \frac{\hbar^2(l + \frac{1}{2})^2}{2\mu R^2} \\ 1, & \text{for } \epsilon \geq B + \frac{\hbar^2(l + \frac{1}{2})^2}{2\mu R^2} \end{cases} \quad (5)$$

The *s*-wave barrier is denoted by B , the moment of inertia by \mathcal{I} , and the reduced mass by μ .

To obtain the angular correlation function $W_{J_0, \mathcal{I}T}(\varphi_{c.m.}^*)$, he integrates Eq. (2) and gets the simple equation

$$W_{J_0, \mathcal{I}T}(\varphi_{c.m.}^*) \propto \exp(\beta_2 \sin^2 \varphi_{c.m.}^*), \quad (6)$$

where

$$\beta_2 = \frac{\hbar^2(J_0 + \frac{1}{2})^2}{2\mathcal{I}T} \frac{\mu R^2}{\mathcal{I} + \mu R^2}. \quad (7)$$

In the same spirit one can obtain via Eq. (2) the mean channel energy $\langle \epsilon \rangle$ as a function of $\varphi_{c.m.}^*$.

$$\langle \epsilon \rangle = C + D \sin^2 \varphi_{c.m.}^*, \quad (8)$$

where

$$C = B + T + \left[\frac{\mathcal{I}}{\mathcal{I} + \mu R^2} \right] T \quad (9)$$

and

$$D = \frac{\hbar^2(J_0 + \frac{1}{2})^2}{2} \frac{(\mu R^2)}{(\mathcal{I} + \mu R^2)^2} = \beta_2 T \left[\frac{\mathcal{I}}{\mathcal{I} + \mu R^2} \right]. \quad (10)$$

The weighted average of $\langle \epsilon \rangle$ over all angles $\varphi_{c.m.}^*$ gives the overall mean channel energy $\langle \langle \epsilon \rangle \rangle$ predicted for singles measurements (for $\theta_{c.m.} \approx 90^\circ$):

$$\langle \langle \epsilon \rangle \rangle = C + D \left\{ \left[\sum_{n=0}^{\infty} \frac{\beta_2^n}{n!} \frac{(2n-1)!!(2n+1)}{(2n)!!(2n+2)} \right] \left[\sum_{n=0}^{\infty} \frac{\beta_2^n}{n!} \frac{(2n-1)!!}{(2n)!!} \right]^{-1} \right\}. \quad (11)$$

The angular distribution for singles measurements with respect to the beam axis was obtained by Døssing by summing Eq. (2) over all orientations of \vec{J}_0 perpendicular to this axis:

$$W_{J_0, \mathcal{I}T}(\theta_{c.m.}) \propto \exp(-\frac{1}{2}\beta_2 \sin^2 \theta_{c.m.}) I_0(\frac{1}{2}\beta_2 \sin^2 \theta_{c.m.}). \quad (12)$$

With these equations we can now analyze our data in several different ways to test for equilibration. The spectra in singles can be used along with β_2 from Eq. (6) and Eqs. (1) and (9)–(11) to obtain the parameters B and T . The singles angular distributions can be used with Eq. (12) to give an independent value of β_2 . The spectra and angular correlations in coincidence can also be used with Eqs. (8)–(11) to give a consistency check on the value of B . If these various parameters are mutually consistent then we can estimate the root-mean-square spin of the emitter J_{rms} and the Fermi gas level density parameter “ a .” Also the barrier to evaporation B can be compared to that for fusion to give a probe of the effects of deformation.¹⁷ Of course, these evaporated particles may be emitted over several steps of the emission cascade; hence, the nuclear parameters should be considered as effective averages.

D. Analysis of the results with the assumption of thermal equilibration and evaporation prior to scission

The various experimental quantities we have measured are given in Table I and in Figs. 8–11. The various quantities derived from these data by means of the equations just discussed are given in Table II. Let us begin with the analysis of the singles studies and then turn to those from coincidence measurements.

Some of the spectra for ^4He obtained in singles are shown in Figs. 8 and 9. It is clear that an uncertain fraction of the particles have been eliminated by the experimental threshold. This loss is not very important for the estimate of T' via Eq. (1) but will obviously affect the mean energy $\langle \langle \epsilon \rangle \rangle$ and the associated value of B from Eqs. (9)–(11). We choose for the moment to accept this systemat-

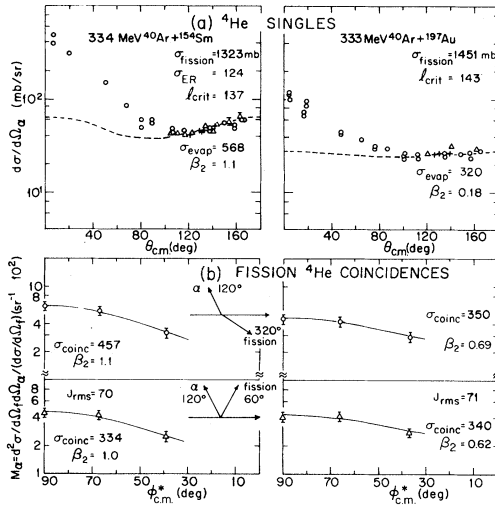


FIG. 10. (a) Measured angular distributions for ${}^4\text{He}$ in the singles mode from Refs. 7 and 8 (separate experiments indicated by different symbols). The decomposition of the evaporative component is shown by a dashed line [least squares fit of Eq. (12)]. Also given are the related cross sections I_{crit} and β_2 values as taken from the singles data (see Table II). (b) Out-of-plane correlations are shown from this work with solid lines indicating least-squares fits to Eq. (6). Also shown are the resulting values of β_2 , J_{rms} , and the corresponding integrated coincidence cross sections σ_{coinc} .

ic overestimate of $\langle\langle\epsilon\rangle\rangle$ and B so as to get a consistent set of values for comparison of singles and coincidence data. From Eq. (1) and a preliminary value of B from Ref. 17 (B_{fusion}) we obtain values of T'_1 by fitting to the high energy tail of the measured singles spectra. These values of B and T' were refined by iterative estimates of B from Eqs. (9)–(11) followed by reestimation of T' from Eq. (1); the resulting values of B and T'_2 are given in the upper section of Table II. This iteration involved the use of (a) the mean energies, Eqs. (9)–(11), (b) the values of β_2 from the coincidence data to be discussed next, and (c) the approximation that values of T' from the spectral shapes can be identified with T in the expression for β_2 . Also, we must estimate the ratio $\mathcal{J}/(\mathcal{J}+\mu R^2)$; as discussed in Sec. III E, we take \mathcal{J} for a spherical nucleus. Clearly, this gives only an approximation to the ratio $[\mathcal{J}/(\mathcal{J}+\mu R^2)]$, but this plays a rather minor role here.

Next, turn to the angular distribution in singles as shown in the upper parts of Figs. 10 and 11. They result from three different experiments as shown by the different symbols. As we were not satisfied with the precision of the β_2 values ex-

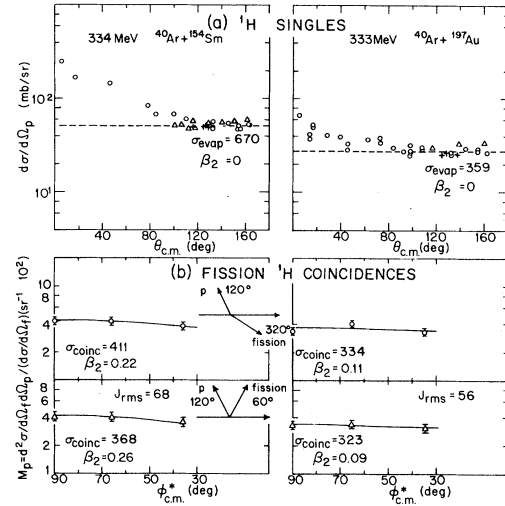


FIG. 11. Same as Fig. 10 for ${}^1\text{H}$.

tracted from the singles data in Ref. 7, many of those measurements were repeated under better conditions.⁸ In Ref. 8 the new results will be compared to the former ones and weighted averages will be given and discussed; in Figs. 10 and 11 and Table II we give cross sections and β_2 values from these weighted averages. As described in Ref. 7 these distributions (for $\theta_{\text{c.m.}} > 120^\circ$) were fit to Eq. (12) to obtain the values of β_2 as shown in Table II (upper). In each case the new values of β_2 are smaller than those reported earlier; this leads to small changes in the angle-integrated cross sections. (The complete angular distributions including the forward-peaked components are shown for completeness in Figs. 10 and 11.) Let us now identify the parameters β_2 as obtained from the coincidence data from this work and then discuss the overall consistency of the various values of β_2 and J_{rms} .

The coincidence data are analyzed here with the assumption that the spin vector of the emitter is exactly perpendicular to the reaction plane. We feel that this is a very good approximation, as discussed in detail in Appendix A. The lower parts of Figs. 10 and 11 show the coincidence multiplicities as a function of the c.m. angle $\phi_{\text{c.m.}}^*$ with respect to the spin vector. By fitting these data to Eq. (6) we obtain the values of β_2 shown in the figures and listed in Table II (for coincidence studies). For ${}^{116}\text{Sn}$ and ${}^{154}\text{Sm}$ the value of β_2 from the coincidence data is essentially consistent with that inferred from the singles data. One might expect that the coincidence requirement with fission might single out the higher spin systems for the ${}^{116}\text{Sn}$ and ${}^{154}\text{Sm}$ reactions. This would lead one to

TABLE II. Quantities derived from singles and coincidence data for reactions of 333 MeV $^{40}\text{Ar} + X$.

	^{197}Au		^{154}Sm		^{116}Sn	
	^4He	^1H	^4He	^1H	^4He	^1H
Results from studies in singles mode						
T'_1 (MeV) ^a	2.5 ± 0.1	2.1 ± 0.1	2.6 ± 0.1	2.3 ± 0.2	2.7 ± 0.1	2.1 ± 0.2
T'_2 (MeV) ^b	2.9 ± 0.2	2.5 ± 0.2	3.0 ± 0.2	2.7 ± 0.2	3.2 ± 0.2	2.4 ± 0.1
A/a (MeV) ^c	16.6	11.3	12.3	9.7	11.2	6.7
$\langle \langle \epsilon \rangle \rangle$ (MeV)	24.0 ± 0.3	12.3 ± 0.3	22.1 ± 0.1	11.8 ± 0.1	21.4 ± 0.3	10.8 ± 0.1
B (MeV) ^d	17.4 ± 0.4	7.3 ± 0.2	14.7 ± 0.1	6.2 ± 0.3	11.1 ± 1.3	5.4 ± 0.1
B_{fusion} (MeV) ^e	22.4	12.0	19.2	10.4	17.1	9.4
β_2^f	0.18 ± 0.07	< 0.4	1.1 ± 0.2	< 0.4	1.70 ± 0.70	0.95 ± 0.82
$J_{\text{rms}}^{g,h}$	33	< 89	70	< 82	66	100
σ_{singles} (mb) ^h	320 ± 50	359 ± 55	568 ± 85	670 ± 95	1158 ± 174	1697 ± 254
l_{ER}^h	0		39		68	
l_{crit}^h	143		137		112	
Results from coincidence studies						
$\theta_G = 60^\circ, \theta_S = 120^\circ$						
β_2^i	0.62 ± 0.11	0.09 ± 0.07	1.0 ± 0.1	0.26 ± 0.13	0.6 ± 0.6	0.57 ± 0.16
J_{rms}^j	69	53	68	71	40	74
σ_{coinc}^j	340	323	334	368	117	368
$\theta_G = 320^\circ, \theta_S = 120^\circ$						
β_2^i	0.69 ± 0.07	0.11 ± 0.11	1.1 ± 0.1	0.22 ± 0.12	2.3 ± 0.2	0.30 ± 0.15
J_{rms}^j	73	59	73	65	80	54
σ_{coinc}^j	350	334	457	411	194	393

^aFrom Eq. (1) with $B = B_{\text{fusion}}$ (Ref. 17).^bFrom Eq. (1) with B from $\langle \langle \epsilon \rangle \rangle$ as observed and Eqs. (9)–(11).^cFrom Eqs. (13), (14), and T'_2 .^dFrom $\langle \langle \epsilon \rangle \rangle$, T'_2 [Eqs. (9)–(11)], and β_2 from fits of Eq. (6) to the coincidence data.^eFrom Ref. 17.^fFrom fits of Eq. (12) to singles data.^gFrom β_2 for singles data (f above).^hFrom averages of singles data in Refs. 7 and 8.ⁱFrom fits of Eq. (6) to the coincidence data.^jFrom β_2 for coincidence data (i above).

expect larger values of β_2 from the coincidence data. In addition, lower values of β_2 might result from the singles due to an underestimation of the forward-peaked component in the $90^\circ - 120^\circ$ region. These effects are not apparent for ^{116}Sn or ^{154}Sm , but the latter one may enter for ^4He from $\text{Ar} + \text{Au}$. In any case, we feel that the values of β_2 from the coincidence data are more reliable, and we will use them in the discussion that follows.

From fits to experimental data we have now obtained all the parameters that we can get (i.e., T'_2 , B , and β_2). We can use these parameters to integrate the coincidence cross sections over all angles for both the light charged particles and for the

fissionlike fragments. The equations for these integrations to obtain σ_{coinc} have been given in Ref. 15. The values of σ_{coinc} from our separate coincidence configurations are given in the lower part of Table II; for ^{197}Au they are very close to one another. For ^{154}Sm and ^{116}Sn the values for ^4He from $\theta_G = 60^\circ$ are always smaller than those from $\theta_G = 320^\circ$. This discrepancy can probably be explained by our operational definition of fission in the GT. As shown in Fig. 1 we have cut off the low energy heavy products to avoid targetlike products from deeply inelastic reactions. For $\theta_G = 320^\circ$ the fraction of fissionlike fragments cut out would seem to be negligible (see Figs. 1 and 2);

for $\theta_G = 60^\circ$ we have eliminated a certain fraction of the fissionlike events. This fractional loss is expected to increase from Au to Sm to Sn due to the decrease in kinetic energy of the fission products as compared to our low energy cutoff. With allowance for such a correction (crudely estimated to be $3 \pm 3\%$, $19 \pm 9\%$, and $25 \pm 15\%$ for Au, Sm, and Sn, respectively), we feel that the level of consistency of these coincidence cross sections is acceptable.

The most reliable values of σ_{coinc} are those on the bottom line of Table II. They are larger than those reported in Ref. 7 because the values of β_2 obtained from the coincidence data in this study are smaller than those obtained from the singles data given in Ref. 7. It is interesting that for the ^{197}Au target essentially all the H/He emission at backward angles is in coincidence with fission (little if any is left for quasielastic or deeply inelastic reactions). Also, for the ^{154}Sm target, about $\frac{2}{3}$ of these H/He emissions are in coincidence with fission; the cross sections for evaporation residues and fission imply that fission is dominant for $39 < J < 137$.^{7,8} If H/He evaporation were equally probable for this whole spin zone then J_{rms} would be expected to be ≈ 110 . From the coincidence data we estimate $J_{\text{rms}} = 65 - 73$ for ^{154}Sm (by using \mathcal{J} values for nonspherical emitters this estimate could be raised by somewhat). It seems that the spin zone for H/He evaporation extends well into that for the composite systems destined to fission; however, as J_{rms} is less than 110 we infer that the systems of spin approaching $l_{\text{crit}} (\approx 137)$ give relatively fewer evaporated H/He. This conclusion is consistent with the systematics of the cumulative decay fractions of Ref. 10.

Finally, the overall consistency can be tested via the mean energies as shown in Fig. 12. We have

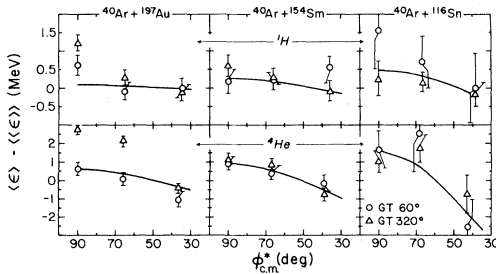


FIG. 12. Mean energy in coincidence mode $\langle \epsilon \rangle$ minus that in singles mode $\langle \langle \epsilon \rangle \rangle$ vs out-of-plane angle $\phi_{\text{c.m.}}^*$. Smooth curves are calculated from Eqs. (8) and (11) with parameters given in Table II as discussed in the text.

chosen to plot the difference between mean energies in coincidence and those in singles, $\langle \epsilon \rangle - \langle \langle \epsilon \rangle \rangle$. Values for each were determined in the same telescope with the same energy calibrations and thresholds. In this way we hope to cancel small systematic errors and get the best precision. Figures 8 and 9 show the energy spectra along with the energy cuts used for some of the cases. Note, however, that separate mean energies in singles have been used for each separate telescope (not the overall average).

The smooth curves in Fig. 12 were derived from Eqs. (8) and (11) with the β_2 values (from coincidence data), the value of T set equal to T'_2 from Table II, and the estimate of $\mathcal{J}/(\mathcal{J} + \mu R^2)$ as discussed in the next section. With the exception of several points from ^{197}Au the consistency is within experimental errors. The discrepant points might be accounted for by a small contribution ($\approx 10\%$) of evaporative emission from the fragments. The sensitivity of the mean energy to emission from the fragments is indeed highest in this geometry for the Au target. We will discuss this further in another paper.⁸

E. Relationship of the derived level density parameters to those from the statistical model and the barrier parameters to those from fusion cross sections

It would appear that the overall pattern of these results is essentially consistent with particle evaporation from a thermally equilibrated composite system. If this is the case, then, it is interesting to examine the significance of the derived quantities in terms of the statistical properties of the emitting complex. From Eq. (7) and the values of β_2 and T (approximated by T'_2) one can estimate $\langle (J_0 + \frac{1}{2})^2 \rangle^{1/2}$ or J_{rms} . For μR^2 we take values from systematics of fusion cross sections as discussed in Refs. 15 and 17 [$\mu R^2 = \mu(r_0 A^{1/3} + R_p$ or $R_\alpha)^2$ with $r_0 = 1.41$ fm, $R_p = 1.44$ fm, and $R_\alpha = 2.53$ fm]. For the moment of inertia we use that of a rigid sphere of radius $1.2A^{1/3}$ fm. Deformation of the emitter may well lead to substantially larger values of \mathcal{J} for the real situation; hence, we may underestimate J_{rms} by this choice. The various estimates of J_{rms} are listed in Table II. They are all quite large and are similar for each target. As discussed above we feel that the values of J_{rms} from the coincidence data are more reliable, and it is these values we use in the discus-

sions below.

One can use the values of the temperature T'_2 to infer the Fermi gas level density parameter a . The most simple approximation is to set the spectral parameter from Eq. (1), T'_2 , equal to T and to assume first-step evaporation. Then we have

$$E_{\text{th}} = aT^2, \quad (13)$$

where

$$E_{\text{th}} = E^* - \hbar^2 J_{\text{rms}}^2 / 2\mathcal{I} \quad (14)$$

(i.e., the thermal energy E_{th} is the total excitation energy E^* corrected for rotational energy). In the upper part of Table II we give these simple estimates of a expressed as A/a (normally, one expects $a = A/\text{constant}$). These values of A/a in Table II are very similar for each target but for ${}^4\text{He}$ and ${}^1\text{H}$ there seems to be a small but systematic difference. They are also quite similar to values used commonly to account for evaporation at lower excitation energies ($\approx 8-10$ MeV).²⁷

The evaporation barriers B in Table II are probably overestimates for two reasons: (1) No correction has been made for the low energy particles lost because of the detection threshold; and (2) Equation (11) was derived with the sharp cutoff approximation for the transmission coefficients.

We have also used the program GROGIF to calculate the shapes of the ${}^1\text{H}$ and ${}^4\text{He}$ spectra.²⁸ A comparison of $\langle\langle\epsilon\rangle\rangle$ and T' for the measured and GROGIF spectra removes the two problems mentioned above. These calculations have been made with $a = A/10$ MeV⁻¹ and with Hill-Wheeler transmission coefficients as described in Ref. 17. The results are listed in Table III. Clearly, the evaporation barriers from Table II give calculated mean energies $\langle\langle\epsilon\rangle\rangle$ that are much closer to the experimental values than those calculated using fusion barriers. (One could obtain a more refined set of barrier parameters by searching for a better fit, but that is not our purpose here.) The T' parameters from the calculated spectra [obtained by fitting Eq. (1) to the calculated spectra in the same way as for the experimental data] are close to those observed; also, the difference between T' for ${}^1\text{H}$ and ${}^4\text{He}$ is reproduced by the calculation. One might conclude that the level densities of those highly excited nuclei are reasonably well described by the Fermi gas formula with a values similar to those at low energies. The mean energies, however, demand emission barriers much smaller than those for fusion.¹⁷ The obvious inference is that these high spin emitters are strongly deformed. In the case of ${}^{237}\text{Bk}$, fissionlike breakup follows essential-

TABLE III. Comparison of observed values of T' and $\langle\langle\epsilon\rangle\rangle$ (in MeV) to those calculated (GROGIF) for first step evaporation.

	${}^{237}\text{Bk}^*$		${}^{194}\text{Hg}^*$		${}^{156}\text{Er}^*$	
	${}^4\text{He}$	${}^1\text{H}$	${}^4\text{He}$	${}^1\text{H}$	${}^4\text{He}$	${}^1\text{H}$
Observed quantities from Table II						
T'_1	2.5	2.1	2.6	2.3	2.7	2.1
T'_2	2.9	2.5	3.0	2.7	3.2	2.4
$\langle\langle\epsilon\rangle\rangle$	24.0	12.3	22.1	11.8	21.4	10.8
Calculated quantities from GROGIF ^a						
$a = A/10$ MeV ⁻¹ , $B_{p,\alpha}$ from fusion (Ref. 17), compare to T'_1 above						
T'^b	2.7	2.4	3.3	3.0	3.5	3.4
$\langle\langle\epsilon\rangle\rangle^c$	27.7	16.0	26.3	15.3	27.0	15.0
$a = A/10$ MeV ⁻¹ , $B_{p,\alpha}$ from Table II, compare to T'_2 above						
T'^b	2.7	2.4	3.2	3.0	3.5	3.4
$\langle\langle\epsilon\rangle\rangle^c$	22.8	11.7	22.1	11.7	22.6	11.7

^aInput spin in GROGIF set to J_{rms} from Table II.

^bObtained by fit of Eq. (1) to the high energy tail of the calculated spectrum ($\frac{1}{2}$ to $\frac{1}{20}$ of the maximum) in the same way as for the experimental data (Ref. 8).

^cObtained with the same low-energy cutoff as used for the experimental data.

ly all the evaporative decay and one might suspect that its evaporation was sampling all the shapes of the composite system between contact and scission. As the scission point might be highly deformed (surely much more deformed than the saddle point), the effective evaporation barriers might be greatly reduced in comparison to fusion. By contrast, it is quite interesting that very small evaporation barriers have also been inferred¹⁷ for the reaction 121 MeV $^{12}\text{C} + ^{182}\text{W}$ ($E^* = 98$ MeV, $l_{\text{crit}} = 45$), where $< 5\%$ of the H/He evaporation is accompanied by fission.²⁹ It would seem that substantial deformation is a common aspect of evaporative emission in many heavy ion reactions whether accompanied by fission or not.

F. Statistical model calculations

In this study and in Refs. 7–10 an extremely large data base has been presented which can provide many constraints on a theory of statistical decay. A detailed set of statistical-model calculations is beyond the scope of this paper. However, many interesting aspects of statistical decay (expectations for evaporative cross sections and J_{rms} values) can be revealed by semiquantitative comparison of the experimental data to E - J field maps as shown in Figs. 13–15. (We use the codes EMIK and GROGIF²⁸; both are modifications of GROGI-2.³⁰) To assist in these comparisons we give in Table IV an

abbreviated set of the cumulative decay fractions from Refs. 7–10. The calculated field maps give first-step decay fractions for each compound nucleus. Table IV gives cumulative decay fractions for all steps of the evaporation cascade. Comparison of the two requires that the reader locate the position in E^* - J space on Figs. 13, 14, or 15, corresponding to a given initial value of $E^* - l_{\text{crit}}$ in Table IV. Then one must make a rough mental integration of a hypothetical chain of individual decay fractions corresponding to the individual steps in the decay chain of the compound nucleus. Let us consider one case at a time.

1. The compound system $^{237}\text{Bk}^*$

From Table IV we see cumulative decay fractions of 0.061 and 0.036 for ^1H and ^4He , respectively, from $^{237}\text{Bk}^*$ for $E^* = 64$ MeV, $l_{\text{crit}} = 68$. In Fig. 13(a) we note that the first step decay fractions for ^1H and ^4He are both less than 1% for all points of the map with $E^* < 70$ MeV. Thus, it seems unlikely that even the sum of decay fractions for several steps could give the total needed to match the experiment. These calculations were made with all level density parameters equal ($a = A/8$ MeV $^{-1}$) and with evaporation barriers equal to those for fusion. However, the mean energies of ^1H and ^4He , as analyzed in Table II, require considerably smaller barriers to evaporation.

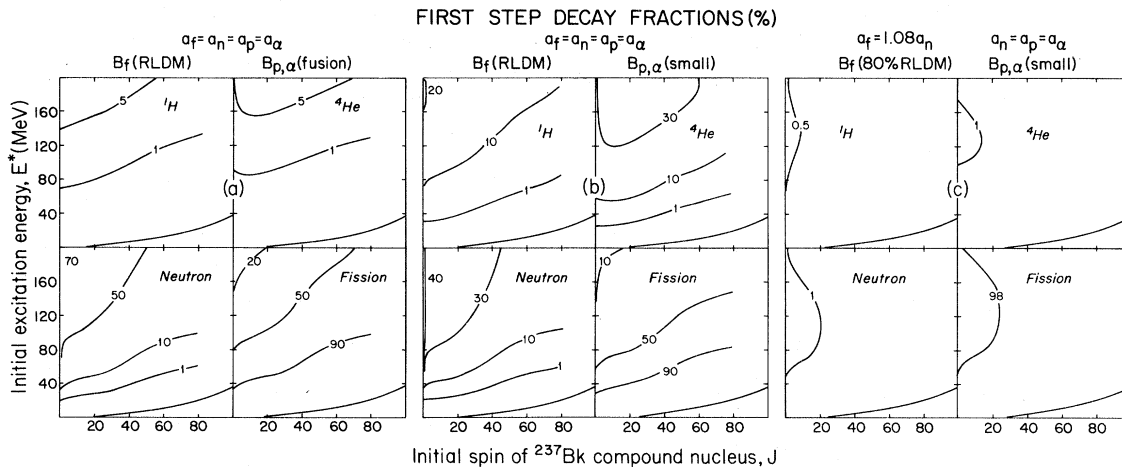
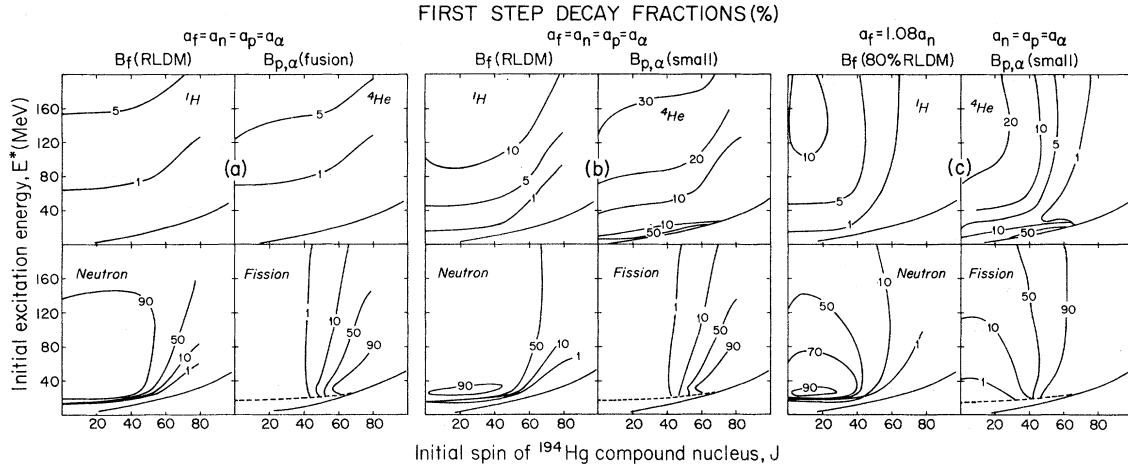


FIG. 13. E^* - J field maps for evaporation probability contours calculated for $^{237}\text{Bk}^*$ with the indicated parameters. (a) All level density parameters are taken to be $A/8$, the fission barrier B_f is taken from the liquid drop model (RLDM) (Ref. 5), and evaporation barriers for ^1H and ^4He $B_{p,\alpha}$ are taken from fusion systematics (Ref. 17). (b) Same as (a) except the evaporation barriers $B_{p,\alpha}$ are taken to be the empirical ones given in Table II. (c) Saddle point level density parameter a_f taken as 1.08 times a_n , fission barriers are 80% of those in Ref. 5 (RLDM), and empirical evaporation barriers given in Table II.

FIG. 14. Same as Fig. 13 for $^{194}\text{Hg}^*$.

In Fig. 13(b) decay maps are presented corresponding to these empirically observed evaporation barriers. Naturally, the H/He evaporation probabilities are enhanced and now the ^4He decay seems to be of the same order as the data in Table IV. Also, the calculated proton emission lags far behind that for alphas for all parts of the map. We see no way to reconcile this to the observations in Table IV.

In Fig. 13(c) another set of parameters is chosen, similar to those in Ref. 31, with level densities enhanced for the fission saddle point [$a_f/a_n=1.08$; $B_f=0.8B_f$ (RLDM)]. This parametrization clearly makes the fission decay so strong that H/He evaporation would be almost completely forbidden. From these evaporation calculations we conclude that the parametrization of Fig. 13(b) is best, but

has a major flaw in its underestimation of proton evaporation.

2. The compound nucleus $^{194}\text{Hg}^*$

From Table IV we see that the observed cumulative decay fractions are 0.12 and 0.076 for ^1H and ^4He , respectively, from $^{194}\text{Hg}^*$ for $E^*=80$ MeV, $l_{\text{crit}}=53$. Figure 14(a) shows calculated first step decay fractions for ^1H and ^4He that are considerably smaller. As for $^{237}\text{Bk}^*$, however, we know that the evaporation barriers (Table II) must be reduced compared to fusion barriers if one is to account for the observed mean energies (see Table III). Figure 14(b) shows decay maps corresponding to the observed evaporation barriers from Table II.

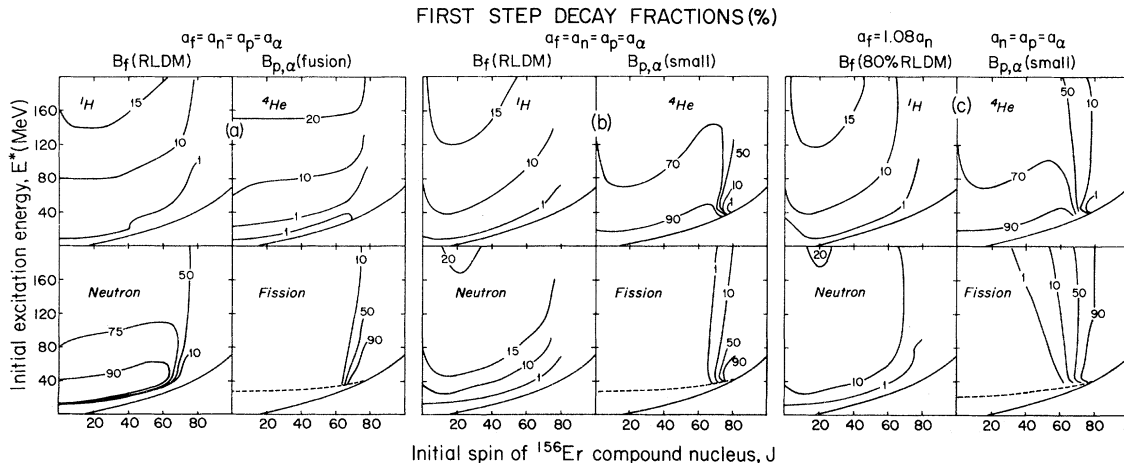
FIG. 15. Same as Fig. 13 for $^{156}\text{Er}^*$.

TABLE IV. Some measured decay fractions.

		Cumulative decay fractions (CDF) ^a			
E^* (MeV)	l_{crit}	^1H	^4He	ER	Fission
$^{237}\text{Bk}^*$					
64	68	0.061	0.036		1.00
107	94	0.13	0.12		1.00
161	149	0.24	0.23		1.00
$^{194}\text{Hg}^*$					
80	53	0.12	0.076	0.31	0.69
80	66	0.093	0.062	0.16	0.84
100	83	0.087	0.092	0.10	0.90
141	101	0.24	0.23	0.08	0.92
194	85	0.98	0.81	0.19	0.81
195	142	0.45	0.40	0.08	0.92
$^{156}\text{Er}^*$					
75	65	0.65	0.28	0.77	0.23
102	77	0.76	0.38	0.51	0.49
141	86	1.14	0.66	0.40	0.60
190	112	1.51	1.03	0.37	0.63

^aCDF_{*i*} is the cross section for *i*th exit channel divided by the fusion cross section. These values were taken from Refs. 7 and 10.

As before, the alpha evaporation fractions are enhanced to a reasonable magnitude, but the proton decay is still too weak. In addition the fission decay [Fig. 14(b)] is localized to $J \gtrsim 50$, which would not be sufficient for the fission data in Table IV.

For Fig. 14(c) we have enhanced the level densities for fission by reducing the fission barriers to 80% compared to RLDM and by increasing the level density parameter, $a_f = 108a_n$. This alteration³¹ makes fission decay dominant for most of the map and confines particle evaporation to the low J regions. The experimental values of J_{rms} in Table II and the decay fractions in Table IV are both inconsistent with such calculated results.

For $^{194}\text{Hg}^*$ we are faced with a twofold dilemma: (a) The calculated ratio of ^1H to ^4He is too small, and (b) it is difficult to get enough fission without making H and He evaporation too small.

3. The compound nucleus $^{156}\text{Er}^*$

Figure 15(a) as compared to Table IV shows the same pattern for $^{156}\text{Er}^*$ as that discussed above for $^{194}\text{Hg}^*$. The calculated decay fractions for ^1H , ^4He , and fission are all too weak. Figure 15(b) shows decay maps corresponding to the smaller

evaporation barriers taken from Table II. Here we have a threefold problem: (a) The calculated ratio of ^1H to ^4He is too small, (b) the fission decay is confined to only the very highest spin zone, and (c) the calculated alpha evaporation is much too strong. Enhancement of the saddle-point level density³¹ [Fig. 15(c)] can improve the comparison for fission decay, but problems (a) and (c) above remain unsolved.

4. Implications for the statistical model

The combination of measured energy spectra, angular distributions, and integrated cross sections for evaporated H and He are difficult to reconcile with the conventional statistical model. The shapes of the energy spectra imply nuclear level densities very similar to those inferred from experimental studies at lower excitation energies. The barriers to evaporation as taken from the spectra are, however, considerably smaller than those from fusion.¹⁷ These small barriers are interesting in several ways: (a) They provide a reflection of the deformations of the compound or composite system during its decay, and (b) they demand recognition in any model calculation based on statistical evaporation.

If we make evaporation calculations that employ these very low barriers, certain contradictions appear in the comparisons to experimental data: (a) The observed ratios of ^1H to ^4He are much greater than those calculated. (b) The calculated alpha particle multiplicities for $^{156}\text{Er}^*$ are much larger than those observed. It seems to us that the data are asking for the inclusion of some new physics in the statistical model of decay at high energies. The available phase space is surely an important driving force but seems to need supplementation possibly in the form of reaction dynamics such as the intrinsic decay rates for ^1H and ^4He emission¹⁰ as compared to the rate of shape evolution from impact to scission.

IV. SUMMARY

We have presented data on the energy and angular correlations of evaporative H and He with respect to fissionlike fragments in reactions of 333 MeV ^{40}Ar with ^{116}Sn , ^{154}Sm , and ^{197}Au . Emission occurs predominantly from the composite system before acceleration of the fragments. The qualitative features of the results resemble ordinary evaporation from a long-lived compound nucleus even though entrance channel partial waves of $l \gtrsim 80$ must be involved. The energy spectra imply temperatures of about 2.5 MeV in reasonable accord with expectations for a completely equilibrated system. They also imply Coulomb barriers 20–30 % lower than those obtained from the systematics of fusion of H or He with targets in their ground states. We gather that the emitting systems are quite deformed compared to those studied in fusion reactions. Evaporation theory has provided several independent ways to infer values of the mean squared spin of the emitter divided by its moment of inertia. The general consistency of the values of J_{rms} obtained by these separate routes gives us added confidence in the applicability of the equilibrium theory. These values of J_{rms} are ≈ 40 –80 or only slightly smaller than $l_{\text{crit}}/\sqrt{2}$ for fusion regardless of the fissility of the system. Our inference is that the particle motions mix the thermal energy much more rapidly than the system moves to the scission point. Such rapidity of equilibration for the particles can be very significant for reaction models and for our overall picture of the flow of energy and angular momentum in heavy ion reactions.

ACKNOWLEDGMENTS

H. Delagrangé has been very helpful with many of the computer codes used in this work; C. Ellsworth prepared the Sn and Sm targets. We appreciate the many helpful actions of the Lawrence Berkeley Laboratory and particularly those of the operating staff of the SuperHILAC. Stimulation and constructive criticism from L. Vaz, L. Kowalski, and M. Kildir are also appreciated. This work was supported in part by the Division of Nuclear Physics of the U. S. Department of Energy and by CNRS of France.

APPENDIX A

For the purposes of this paper we have assumed that the spin vector of the compound (or composite) nucleus is essentially perpendicular to the “reaction plane.” This plane was selected in turn by the direction of the beam and that of the detector for fissionlike products. Let us examine the approximations and assumptions involved in these presumptions. We have presented evidence in Figs. 3–6 and in Refs. 7–10 that ^1H and ^4He emission occur prior to fission. Also, we have presented evidence that the bulk of the ^1H and ^4He emission at $\theta_S = 120^\circ$ is from an evaporation mechanism. Therefore, we have adopted Eq. (6) from the statistical evaporation model for the angular correlation of ^1H and ^4He with respect to the spin vector of the emitting complex. After this evaporative emission (and any additional prefission emission), the reaction system undergoes fission. If this fission process can be described by equilibrium theory, then its angular correlation with respect to the spin vector can also be described approximately by Eq. (6) (Ref. 32) with β_2 replaced by β_f , where

$$\beta_f = \frac{\hbar^2(J_0 + \frac{1}{2})^2}{2\mathcal{I}_{\text{eff}}T} = \frac{(J_0 + \frac{1}{2})^2}{2K_0^2}. \quad (\text{A1})$$

From the systematics of fission angular distributions one can estimate values of K_0^2 for these reactions.^{33,34} The resulting values of β_f are $\gtrsim 10$ and $\gtrsim 16$ for ^{197}Au and ^{154}Sm , respectively. The large value of β_f for ^{154}Sm implies $\lesssim 8^\circ$ for a mean tilt angle of the reaction plane away from the normal to the spin axis. The resulting increase in β_2 values¹⁶ would be less than 4% and would not alter the consistency between singles and coincidence data.

To test this idea we have written a Monte Carlo

computer code to simulate this situation. The angular correlation of evaporated particles has been chosen as the result of two separate weighting functions: (1) First, the tilt angle of the spin vector (with respect to the reaction plane) was chosen from Eq. (6) with β_f taken from fission systematics, and (2) then the evaporation angle with respect to the spin vector was chosen from Eq. (6) with β_2 taken from Table II. The resultant calculated out-of-plane correlations show only small differences from those calculated for unperturbed evaporation.

One may also consider the effect of kicks to the fission fragment direction due to particle evaporation either before or after the fission event. This smearing could be estimated by calculations or simply taken from measurements of the out-of-plane correlations between two fission fragments. Such correlations have been measured³⁵ for 340 MeV $^{40}\text{Ar} + ^{197}\text{Au}$; they give a full width at half maximum of about 8° . This effect is of the same order as that considered above.

We conclude that (if the fission processes here follow the systematics of K_0^2 established at lower energies) the tilt angle of the spin vector from the reaction plane has only a very small effect on the out-of-plane correlation for H or He.

APPENDIX B

Measurements of angular distributions for reaction products with continuous spectra require particular attention to the technicalities of the transformations from laboratory to the center of mass. If both mass and velocity of the detected fragment are known (as well as the velocity of the c.m.) then the transformation can be unambiguously performed event by event. Then, the problem centers on the angular binning of the events in the c.m. and whether or not the extent of the observation angles was sufficient to avoid biases to the results. This paper involves observations of H and He which present continuous spectra for products of known mass. In addition it involves fission products for which we measure the energy spectra but for which we have not determined the individual masses. The transformation of interest to us is from laboratory to the center of mass for the reaction (not to the frame of a moving fission fragment); hence, the velocity of the moving frame is uniquely known.

The transformation for H and He products presents no particular confusion for two reasons: (a) The observed velocities of H/He are all larger

than that of the c.m., and (b) the energy spectra for H/He vary rather slowly with angle. We perform the transformation uniquely (event by event) and examine the range of c.m. angles corresponding to a given laboratory configuration. As this angular range is small with respect to that for significant spectral change, we treat the resulting c.m. energy spectrum as if it were localized at the average c.m. angle.

The fission products present quite a different problem for two reasons: (a) The masses (and therefore the velocities) are not known event by event, and (b) the energy spectra are very broad and the velocities for the heavier fragments are comparable to the c.m. velocity. In spite of these problems it is common to treat each event as if it corresponds to the unique mass of a symmetric fission fragment and proceed as described above (see Ref. 34, for example). This approximation is quite acceptable if the velocity spectra are not too broad. However, fissionlike products are known to have very broad mass distributions in reactions involving high energy and angular momenta. Therefore, their velocity spectra are also broad, and some of the heavy fragments may have velocities in the c.m. smaller than the velocity of the c.m.

To address this problem we proceed in two steps: (a) First, we make a tentative transformation to the c.m. with the approximation of uniquely symmetric fission as described above, and (b) then, we use a Monte Carlo kinematic simulation

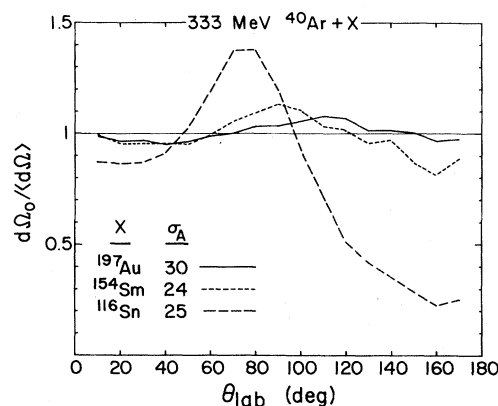


FIG. 16. Ratio of solid angles in the c.m. system for fission products from the indicated reactions. The quantity $d\Omega_0$ was obtained with the approximation of fission to a unique product (symmetric fission) with a unique total kinetic energy (TKE) release. The quantity $\langle d\Omega \rangle$ was obtained (by Monte Carlo calculation) with a Gaussian distribution of mass A and TKE (σ_A as indicated; $\langle \text{TKE} \rangle$ from Ref. 21; $\sigma_{\text{TKE}} = 15$ MeV).

to estimate a correction factor for the effect of the width of the velocity distribution. This correction factor is shown in Fig. 16 for the reactions of interest here.

As we want to transform the energy integrated cross section, the Jacobian is simply the ratio of the solid angle in the laboratory to that in the c.m. Therefore, the correction factor we seek is simply the ratio of the c.m. solid angle $d\Omega_0$ for the unique symmetric product to that for the solid angle $\langle d\Omega \rangle$ averaged over the simulated distribution of velocities. We determine this ratio by comparing the output from two separate Monte Carlo calculations. First, we assume isotropic fission from a

compound nucleus with a unique total kinetic energy (TKE) release and a uniquely symmetric mass. Second, we assume isotropic fission from a compound nucleus, but we include Gaussian distributions of TKE ($\sigma_{\text{TKE}} = 15$ MeV) and of mass A with σ_A values shown in Fig. 16. The numbers of hypothetical fission products were binned versus laboratory angle and the resulting ratios are shown in Fig. 16. These ratios were then used as multiplicative correction factors to the tentative transformations described above. These corrections are most significant for the compound systems of lower Z which have larger numbers of low-velocity fragments.

*Permanent address: Institut de Physique Nucléaire, B. P. No. 1, 91406 Orsay, France.

¹See, for example, D. Agassi, C. M. Ko, and H. A. Weidenmüller, *Ann. Phys. (N.Y.)* **107**, 140 (1977); C. M. Ko, D. Agassi, and H. A. Weidenmüller, *ibid.* **117**, 237 (1979).

²U. Schröder and J. R. Huizenga, *Annu. Rev. Nucl. Sci.* **27**, 465 (1977); V. V. Volkov, *Phys. Rep.* **44C**, 93 (1978).

³W. Norenberg and C. Riedel, *Z. Phys. A* **290**, 335 (1979); C. Grégoire, R. Lucas, C. Ngô, and B. Schurmann, and H. Ngô, *Nucl. Phys.* **A361**, 443 (1981); W. J. Swiatecki, *Prog. Part. Nucl. Phys.* **4**, 383 (1980); Lawrence Berkeley Laboratory Report LBL 10911, 1980 (unpublished).

⁴C. Lebrun, F. Hanappe, J. F. Lecolley, F. Lefebvres, C. Ngô, J. Peter, and B. Tamain, *Nucl. Phys.* **A321**, 207 (1979); B. Heusch, C. Volant, H. Freiesleben, R. R. Chesnut, K. D. Hildenbrand, F. Pühlhofer, W. F. W. Schneider, B. Kohlmeier, and W. Pfeffer, *Z. Phys. A* **288**, 391 (1978); B. Borderie, M. Berlinger, D. Gardes, F. Hanappe, L. Nowicki, J. Peter, B. Tamain, S. Agarwal, J. Girard, C. Gregoire, J. Matuszek, and C. Ngô, *ibid.* **299**, 263 (1981); C. C. Sahm, H. Schulte, D. Vermeulen, J. Keller, H. G. Clerc, K. H. Schmidt, F. Hessberger, and G. Münzenberg, *ibid.* **297**, 241 (1980).

⁵S. Cohen, F. Plasil, and W. J. Swiatecki, *Ann. Phys. (N.Y.)* **82**, 557 (1974).

⁶N. Bohr and J. A. Wheeler, *Phys. Rev.* **56**, 426 (1939).

⁷D. Logan, H. Delagrange, M. F. Rivet, M. Rajagopalan, J. M. Alexander, M. Kaplan, M. S. Zisman, and E. Duek, *Phys. Rev. C* **22**, 1080 (1980).

⁸D. Guerreau, D. Logan, M. F. Rivet, E. Duek, L. C. Vaz, J. M. Alexander, L. Kowalski, and M. S. Zisman (unpublished).

⁹D. Logan, M. Rajagopalan, M. S. Zisman, J. M. Alexander, M. Kaplan, and L. Kowalski, *Phys. Rev. C* **22**,

104 (1980).

¹⁰M. Rajagopalan, D. Logan, J. W. Ball, M. Kaplan, H. Delagrange, M. F. Rivet, J. M. Alexander, L. C. Vaz, and M. S. Zisman, *Phys. Rev. C* **25**, 2417 (1982), the preceding paper; J. M. Alexander, H. Delagrange, M. Rajagopalan, M. F. Rivet, and L. C. Vaz (unpublished).

¹¹T. Ericson, *Adv. Phys.* **9**, 423 (1960).

¹²T. Ericson and V. Strutinski, *Nucl. Phys.* **8**, 284 (1958); **9**, 689 (1959).

¹³L. G. Moretto, *Nucl. Phys.* **A247**, 211 (1975).

¹⁴T. Døssing (unpublished).

¹⁵G. L. Catchen, M. Kaplan, J. M. Alexander, and M. F. Rivet, *Phys. Rev. C* **21**, 940 (1980).

¹⁶W. Kühn, R. Albrecht, H. Damjantschitsch, H. Ho, R. M. Ronningen, J. Slemmer, J. P. Wurm, I. Rode, and F. Scheibling, *Z. Phys. A* **298**, 95 (1980).

¹⁷M. A. McMahan and J. M. Alexander, *Phys. Rev. C* **21**, 1261 (1980); L. C. Vaz, J. M. Alexander, and G. R. Satchler, *Phys. Rep.* **69C**, 373 (1981).

¹⁸See, for example, J. Gilat and J. R. Grover, *Phys. Rev. C* **3**, 734 (1971); M. Blann, *ibid.* **21**, 1770 (1980).

¹⁹M. M. Fowler and R. C. Jared, *Nucl. Instrum. Methods* **124**, 341 (1975).

²⁰J. M. Alexander, H. Delagrange, and A. Fleury, *Phys. Rev. C* **12**, 149 (1975).

²¹V. E. Viola, *Nucl. Data* **A1**, 391 (1966).

²²E. K. Hyde, *The Nuclear Properties of the Heavy Elements III Fission Phenomena* (Prentice-Hall, Englewood Cliffs, New Jersey, 1964).

²³C. Grégoire, M. Berlinger, B. Borderie, D. Gardes, J. Girard, F. Hanappe, J. Matuszek, C. Ngô, and B. Tamain (unpublished), and references therein.

²⁴R. Babinet, B. Cauvin, J. Girard, J. M. Alexander, T. H. Chiang, J. Galin, B. Gatty, D. Guerreau, and X. Tarrago, *Z. Phys. A* **295**, 153 (1980).

²⁵I. Halpern, *Annu. Rev. Nucl. Sci.* **21**, 245 (1971).

²⁶N. Cârjan and B. Leroux, *Phys. Rev. C* **22**, 2008

- (1980).
- ²⁷W. Dilg, W. Schantl, H. Vonach, and M. Uhl, Nucl. Phys. A217, 269 (1973).
- ²⁸H. Delagrange, Centre D'Etudes Nucléaires de Bordeaux-Gradignan Report CENBG 7707, 1977.
- ²⁹J. M. Miller, D. Logan, G. L. Catchen, M. Rajagopalan, J. M. Alexander, M. Kaplan, J. W. Ball, M. S. Zisman, and L. Kowalski, Phys. Rev. Lett. 40, 1074 (1978).
- ³⁰J. R. Grover and J. Gilat, Phys. Rev. 157, 802 (1967); 157, 823 (1967); J. Gilat, Brookhaven National Laboratory Report No. BNL 50246, 1970 (unpublished).
- ³¹F. Plasil, R. L. Ferguson, R. L. Hahn, F. E. Obenshain, F. Pleasonton, and G. R. Young, Phys. Rev. Lett. 45, 333 (1980).
- ³²R. A. Broglia, G. Pollarolo, C. H. Dasso, and T. Døssing, Phys. Rev. Lett. 43, 1649 (1979).
- ³³J. R. Huizenga and R. Vandenbosch, *Nuclear Fission* (Academic, New York, 1973).
- ³⁴P. Dyer, R. J. Puigh, R. Vandenbosch, T. D. Thomas, M. S. Zisman, and L. Nunnolley, Nucl. Phys. A322, 205 (1979).
- ³⁵E. Duek, L. Kowalski, M. Rajagopalan, J. M. Alexander, T. Debiak, D. Logan, M. Kaplan, M. Zisman, and Y. LeBeyec (unpublished).